JOURNAL OF THERMOPHYSICS AND HEAT TRANSFER
Vol. 14, No. 2, April–June 2000

Calculation of Surface Heat Transfer for a Sphere with Wall Injection

Yoshinori Izawa* and Keisuke Sawada†
Tohoku University, Sendai 980-8579, Japan

A computational fluid dynamics method is developed to calculate heat-transfer rate for a sphere with wall injection in hypersonic flow. Attention is paid to exploring the enhanced heat-transfer rate by wall injection. The concept of injection-induced turbulence effect is employed in which the injection flow is assumed to be inherently turbulent. A detailed comparison of the calculated heat-transfer distributions with existing experimental data is carried out. Although the quantitative agreement is not yet accomplished for the entire wall surface, the enhanced heat-transfer rate at the stagnation point is well reproduced, and the higher heating rate in the downstream region is indicated in the calculated results.

Nomenclature

A^+ = constant, 26
B = blowing parameter $[\dot{m}C_p(T_t - T_w)/q_0]$
C_p = specific heat with a constant pressure, J/g-K
D = Van Driest damping function
d = mixing length of turbulence, cm
d_m = limiting mixing length of turbulence at the wall, cm
d_{inj} = mixing length of turbulence caused by the injection flow from the wall surface, cm
M_∞ = freestream Mach number
$\dot{m}$ = local mass addition rate, g/cm^2-s
$\underline{\dot{m}}$ = area-averaged mass addition rate to a given location, g/cm^2-s
$\underline{m}^*$ = mass-flow rate ratio $(\underline{\dot{m}}/\dot{m}_\infty)$
$\dot{m}_\infty$ = freestream mass-flow rate, g/cm^2-s
p = pressure, psi
p_t = total pressure of the wind tunnel, psi
q = local heating rate, W/cm^2
q_0 = theoretical value of the stagnation heating rate for a sphere with 17.78 cm diameter, W/cm^2
R_e = Reynolds number based on the nose diameter
R_N = nose radius, 8.89 cm
s = distance along the wall surface from the stagnation point, cm
T = temperature, K
T_t = total temperature of the wind tunnel, K
u = velocity component tangential to the wall, cm/s
v = velocity component normal to the wall, cm/s
y = distance from the wall, cm
y^+ = dimensionless wall coordinate
η = dimensionless normal coordinate; Eq. (5)
μ = molecular viscosity, g/cm-s
μ_t = eddy viscosity, g/cm-s
$(\mu_t)_{\text{BL}}$ = eddy viscosity evaluated by the Baldwin–Lomax turbulence model, g/cm-s
$(\mu_t)_{\text{inj}}$ = eddy viscosity caused by the injection flow from the wall surface, g/cm-s
$(\mu_t)_{\text{Park}}$ = eddy viscosity of the injection flow at the wall according to Park's model, g/cm-s
ρ = density, g/cm^3
τ = time constant, s
χ = Karman constant, 0.4
Ψ = stagnation point heating rate ratio (q/q_0)
ω = vorticity, 1/s

Subscripts

$B = 0$ = value for no mass addition
e = edge of boundary layer
s = local value at s
w = wall value

Introduction

ACCURATE prediction capability of surface heat-transfer rate for a blunt geometry in hypersonic flows is a necessity for designing space vehicles. Several analytical formulas based on the boundary-layer theory for predicting heat-transfer rate at the stagnation point, such as the one proposed by Fay and Riddell,[1] are available and have been used in past space vehicle designs.

For a space vehicle entering into the atmosphere with a superorbital velocity, it is customary to employ an ablator as a heat shield. Ablative material such as carbon-phenolic absorbs heat by the pyrolysis process. At the same time pyrolysis gas is injected into the boundary layer from the surface.[2] The convective blockage effect of ablation product gas becomes effective if the surface is covered by laminar injected gas, which alleviates temperature gradient and thus reduces the amount of heat being transferred to the surface by conduction.

Although the boundary-layer theory can be extended to include the surface blowing case,[3,4] the prediction of heat-transfer rate for the ablative heat shield has inherent difficulties. A recent paper pointed out that, when ablation occurs, surface heat-transfer rate can be enhanced significantly by turbulence effect that comes either from surface injection flow or spallation.[5] The latter can also enhance radiative heat transfer greatly.

Presently, several sample return space missions such as MUSES-C in Japan[6] and Stardust in the United States[7] are being planned. In the former plan a probe vehicle will travel to the asteroid orbiting near Mars and pick its surface sample. In the latter plan a probe vehicle will go through the tail of a comet and also gather some samples. After picking up samples, these probe vehicles will come back to Earth and enter the atmosphere with velocity exceeding 12 km/s. Because of this higher velocity, those reentry bodies employ ablative materials for heat protection. Particularly in Japan's case, weight of the entry body is critically limited, and thus a thicker ablator cannot be utilized. This requires the sophistication for design procedure of the thermal protection system and motivates the present study.

As just stated, foreign gas injection in the boundary layer can reduce the amount of heat conduction to the surface. However, when

Presented as Paper 99-0734 at the AIAA 37th Aerospace Sciences Meeting, Reno, NV, 11–14 January 1999; received 2 March 1999; revision received 4 October 1999; accepted for publication 4 October 1999.

*Graduate Student, Department of Aeronautics and Space Engineering, Aobayama 01. Student Member AIAA.

†Professor, Department of Aeronautics and Space Engineering, Aobayama 01; sawada@cdf.mech.tohoku.ac.jp. Senior Member AIAA.

turbulence comes out in the boundary layer, the amount of heat being transferred to the surface can be increased. It is well known that the injection of foreign gas in the boundary layer through porous material promotes turbulence particularly in the downstream region, and this increases surface heat-transfer rate considerably. Such a phenomenon is well demonstrated in the experimental study reported by Kaattari.[8] He measured the surface heat-transfer rate for several blunt bodies in hypersonic flows. Using a porous wall, he simulated the effect of ablation. With increasing the amount of injection gas, turbulent transition actually took place in an otherwise laminar boundary layer, and the higher heat-transfer rate was observed in the experimental data. The same tendency was also shown in the experimental study of Feldhuhn.[9]

A theoretical modeling of this phenomenon has already been developed by Park.[10] In an attempt to explain the higher heat-transfer rate at the stagnation point observed in experiments, he conjectured that the injection gas was already turbulent. He derived the functional form for mixing length at the surface and time constants for various porous materials based on the data from relevant experiments. Recently, this idea of injection-induced turbulence was adopted in our previous numerical study, assuming the model could be applied to the region other than the stagnation point. In Ref. 11 the velocity profile in the boundary layer over a spherical blunt body measured in a hypersonic wind tunnel was calculated and compared with the experimental data.[12] The suggestion was made that the development of turbulent boundary layer caused by wall injection could be simulated through using the concept of injection-induced turbulence. In another paper the heat flux for the Pioneer-Venus entry probe was calculated.[13] The heat-transfer rate was increased significantly in the downstream region, while being decreased at the stagnation point when ablation gas was injected. This qualitatively explained the flight data.[14]

In the previous study[11] the injection-induced turbulence model was incorporated in the flow solver through the use of the one-equation turbulence model proposed by Goldberg and Ramakrishnan.[15] In the model the damping function for low-Reynolds-number effect was defined by comparing local eddy size with Kolmogorov scale. The distance from the nearby wall was not used in the model. This feature seemed quite favorable for the present numerical approach because we did not have to worry about the behavior of the near-wall low-Reynolds-number term for the turbulent boundary layer with turbulent foreign gas injection. Note that the viscous sublayer disappears with such turbulent gas injection.

In this study we focus on calculating the heat flux profiles over a spherical blunt body with wall injection in hypersonic flow. We compare the calculated results with the existing experimental data.[8] The numerical approach is then assessed and, if necessary, improved. In the following, we first show the calculated results using the earlier numerical approach, and then give the details of numerical approaches. The improved results are then shown for various cases considered in the corresponding experiment. Finally, the related discussions and conclusions will be stated.

Numerical Methods

Brief Description of the Present Scheme

The governing equations are the Reynolds-averaged axisymmetric Navier–Stokes equations. An ideal gas flow with the constant ratio of specific heats 1.4 is assumed both for the freestream gas and the injection gas. The flowfield is solved by a conventional cell-centered explicit finite volume upwind scheme. The employed numerical scheme is essentially the same as used in our previous work[11] except for the treatment of isothermal porous wall boundary condition. The convection term is solved by one of the advection upwind-splitting method (AUSM-DV) scheme with a shock-fix procedure for removing carbuncle phenomenon.[16] The viscous term is evaluated by central differencing. The source term appearing in the axisymmetric equations is evaluated by cell-averaged values. The equations are integrated in time by the conventional two-stage explicit Runge–Kutta method. A local time stepping is employed for a faster convergence.

Injection-Induced Wall-Turbulence Model

According to Park,[10] the eddy viscosity at the wall with injection flow can be described as

$$\mu_{t_w} = 0.4\rho_w v_w d \tag{1}$$

The mixing length d was identified by comparing with experimental data and was given by

$$d = d_m\{1 - \exp(-\tau v_w/d_m)\} \tag{2}$$

The time constant τ was found to be

$$\tau = 0.02 \tag{3}$$

for sintered stainless steel. The limiting mixing length d_m is given by

$$d_m = 35\left(\frac{\partial y}{\partial \eta}\right)_w \tag{4}$$

where η is defined by

$$\eta = \left[2\rho_e \frac{(\mathrm{d}u_e/\mathrm{d}s)_{B=0}}{\mu_e}\right]^{\frac{1}{2}} \int_0^y \frac{\rho}{\rho_e}\,\mathrm{d}y \tag{5}$$

The boundary condition at the porous wall is imposed by first assuming the pressure gradient normal to the wall is zero. This is approximated by $p_w = p_c$, where p_c denotes the averaged pressure in the computational cell adjacent to the wall. We assume that the wall temperature is the same as that of the injection gas and is given by $T_w = 300$ K (Ref. 8). The density of the injected gas ρ_w is determined from the ideal gas equation of state. The injection velocity at the wall surface is then given by $v_w = \dot{m}/\rho_w$. The foreign gas is assumed to inject perpendicularly from the wall. After finding the boundary-layer edge based on the total enthalpy profile, the limiting mixing length d_m is determined by using Eqs. (4) and (5). The wall eddy viscosity based on the injection-induced turbulence model is then given by using Eqs. (1) and (2). From this wall value one can find the boundary value of the dependent variable for the one-equation turbulence model by solving the relation between the eddy viscosity and the dependent variable iteratively.[11]

Typical Results by the Preceding Numerical Approach

In this study we aim to reproduce the experimental result of Kaattari in which hypersonic flows over several blunt models with surface injection flow were tested.[8] In his experiment pressurized air was injected through a porous wall made of sintered stainless steel for introducing ablation effect. Heat-transfer measurements were made at various locations.

The model geometry considered in this study is a hemisphere with nose diameter 17.78 cm. The freestream Mach number is 7.32, and the Reynolds number based on the nose diameter is about 1.0×10^6. The reservoir temperature is about 800 K, and the pressure is 400–1600 psi. Figure 1 shows a typical example of a structured mesh with 101×151 mesh points. At the shock position mesh lines are clustered to resolve the detached shock wave crisply.

What we have obtained using the same scheme described in the earlier study was rather a poor agreement with the available experimental data. The employed turbulence model was the Goldberg–Ramakrishnan (G–R) model.[15] The flow condition and other parameters for this example (Run 80H1) are shown in Table 1. Figure 2 shows the obtained density contours. Along the wall, a sharp density change is seen corresponding to the edge of injecting gas. Figure 3 shows the corresponding normalized surface heat-transfer profile. The calculated values are normalized by the calculated stagnation-point heat-transfer rate for zero mass addition, whereas the experimental values are normalized by the stagnation-point heat-transfer rate measured in the experiment also for zero mass addition. For zero mass addition cases the calculated value at the stagnation point becomes about 10% larger than that of the experimental value.

Table 1 Flow conditions and parameters considered in the present calculations

Parameter	Value at run						
	77H1	78H1	79H1	80H1	88H1	89H1	95H1
P_t, psi	400	400	400	400	800	800	800
T_t, K	782	793	788	775	761	748	797
M_∞	7.32	7.32	7.32	7.32	7.32	7.32	7.32
$R_e \times 10^{-6}$	1.11	1.05	1.07	1.10	2.29	2.37	2.12
q_0, W/cm^2	9.80	9.83	9.77	9.51	13.13	12.94	14.16
$\dot{m}^*$	0.003	0.007	0.022	0.027	0.004	0.010	0.013

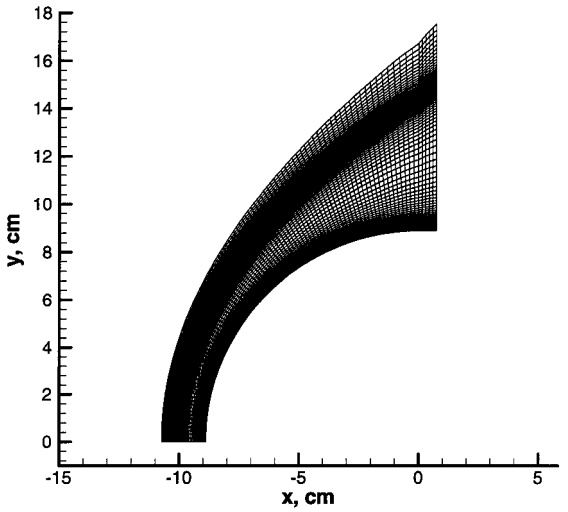

Fig. 1 Computational mesh with 101 × 151 grid points. Mesh lines are clustered to the shock wave as well as in the boundary-layer region.

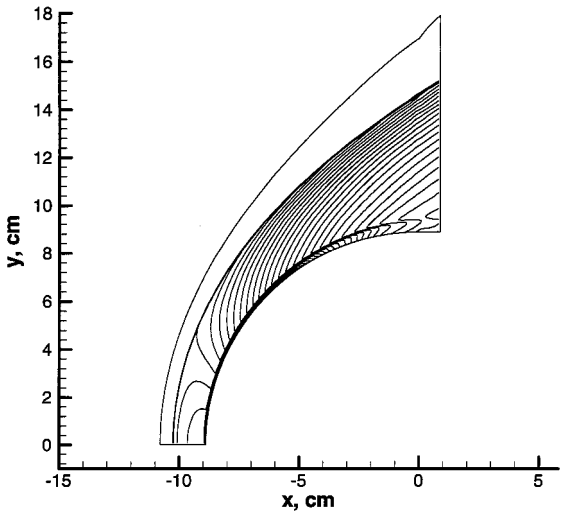

Fig. 2 Typical example of the calculated density contours by the previous method[11] with surface mass addition (80H1). The G–R model is used.[15]

With surface injection one can see the calculated heat-transfer rate at the stagnation point becomes significantly lower than the experiment, while becoming larger in the downstream region. For comparison, the calculated result using the Spalart–Allmaras (S–A) one-equation turbulence model[17] is also shown in Fig. 3. The wall boundary condition is similarly treated as in the G–R model. The heat-transfer rate at the stagnation point decreases and almost coincides with that of the G–R model. Contrary, the peak heating rate at $s/R_N \approx 0.6$ substantially decreases, and a better agreement with the experiment is obtained. Note that the destruction term in the S–A model is inconsistent with the present turbulent injection assumption.

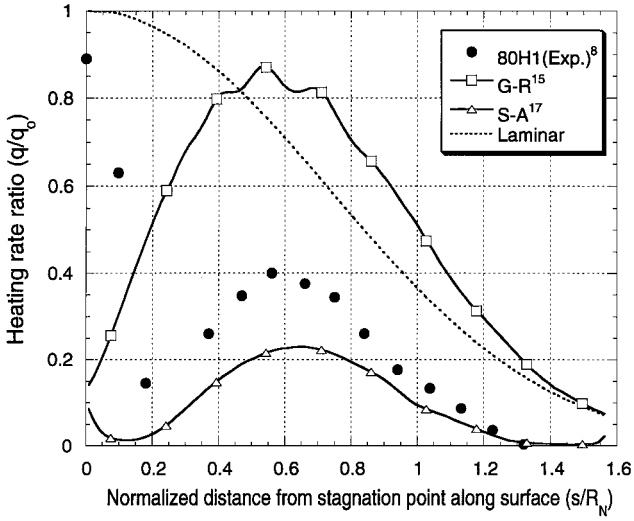

Fig. 3 Typical examples of obtained surface heat-transfer-rate profiles by the previous method.[11]

The preceding results suggest that the turbulence effect caused by the wall injection in the numerical solutions is too small at the stagnation point. This is not acceptable because Park's injection-induced wall turbulence theory was calibrated against the experimental data involving the present one. The suggestion is also made that the calculated heating rate in the downstream region critically depends on the turbulence models.

New Implementation

A proper form of the wall damping function for injection flow was studied by Cebeci.[18] The constant A^+ in the Van Driest damping function[19]

$$D = 1 - \exp(-y^+/A^+) \tag{6}$$

was modified, and a favorable agreement with the experiment was demonstrated. However, in the vicinity of wall, the viscous sublayer region appears, which does not suit with the concept of injection-induced wall turbulence modeling.

The Van Driest damping function is constructed based on the solution for the incompressible Stokes flow over an oscillating flat plate. The amplitude of the oscillation was translated as the fluctuation component of the fluid velocity. In this study the same idea is adopted to construct a wall damping function for turbulent wall injection flow. The eddy viscosity used in the calculation is now assumed in the following form as

$$\mu_t = (\mu_t)_{\text{inj}} + (\mu_t)_{\text{BL}} \tag{7}$$

where the first term in the right-hand side is given by

$$(\mu_t)_{\text{inj}} = \rho d_{\text{inj}}^2 |\omega| \tag{8a}$$

$$d_{\text{inj}} = \max(0, d_w - \chi y) \exp\left(-\frac{y^+}{A^+}\right) \tag{8b}$$

The mixing length d_{inj} takes the maximum value d_w at the wall and decays exponentially in the boundary layer according to the Van Driest theory. The wall mixing length d_w is chosen to satisfy the relation

$$(\mu_t)_{\text{Park}} = \rho_w d_w^2 |\omega_w| \tag{9}$$

The second term in the right-hand side of Eq. (7) is given by the original form of the Baldwin–Lomax algebraic turbulence model.[20] Therefore, the eddy viscosity given by this second term vanishes toward the wall.

Calculated Results by the Modified Method

Improved Results by the New Method

Figure 4 shows the calculated normalized surface heat-transfer rate corresponding to the same conditions for the example shown in Fig. 3. The heating rate at the stagnation point now agrees fairly well with the experimental value. The heating rate in the downstream region, however, becomes too large and almost coincides with that by the G–R model shown in Fig. 3. For comparison, the calculated profile by removing $(\mu_t)_{BL}$ in Eq. (7) is also shown. The heating rate at the stagnation point slightly increases in this case, while it monotonically decreases along the wall surface. This demonstrates the importance of turbulent transition caused by the Baldwin–Lomax model for reproducing the experimental data.

A grid-convergence study is made for this particular case, and the obtained results are indicated also in Fig. 4. One can see that the heat-transfer profile obtained by using the standard mesh (101 × 151) is virtually the same as that given by the finer mesh, although the peak heating in the downstream hump is slightly different. The heat-transfer rate at the stagnation point is almost unchanged. Therefore, the numerical results using the standard mesh can retain a sufficient accuracy for the present investigation.

Seeing the reasonable agreement at the stagnation point, we now consider various cases with varying mass addition rates conducted in Kaattari's experiment.[8] All of the cases considered here are also summarized in Table 1. Calculated cases are chosen for two distinct Reynolds numbers. The variations of mass addition rate along the wall surface for the lower Reynolds number are shown in Fig. 5a, whereas for the higher Reynolds number are in Fig. 5b.

The calculated surface heating profiles for the lower Reynolds numbers are shown in Fig. 6a. One can see that the heating rate at the stagnation point is generally well reproduced, but the heating rate becomes too large in the downstream region. The situation is found to be the same for the higher-Reynolds-number cases shown in Fig. 6b. Note that, for both Reynolds numbers, the response of the heating rate to the variation of mass addition rate is favorably reproduced. With an increasing mass addition rate the heating rate at the stagnation region decreases. In the downstream region a hump in the heating-rate profile becomes evident, although the calculated transition location only slightly moves toward downstream.

At the stagnation point the calculated eddy viscosity always takes the maximum value $(\mu_t)_{inj}$ at the wall, and monotonically decreases toward the edge of the boundary layer because $(\mu_t)_{BL}$ is almost zero. Contrary, in the downstream of the transition point, the maximum value of the eddy viscosity occurs in the middle of the boundary layer. The eddy viscosity profile is obviously affected by the growth of $(\mu_t)_{BL}$, which is triggered by the introduction of $(u_t)_{inj}$ from the wall.

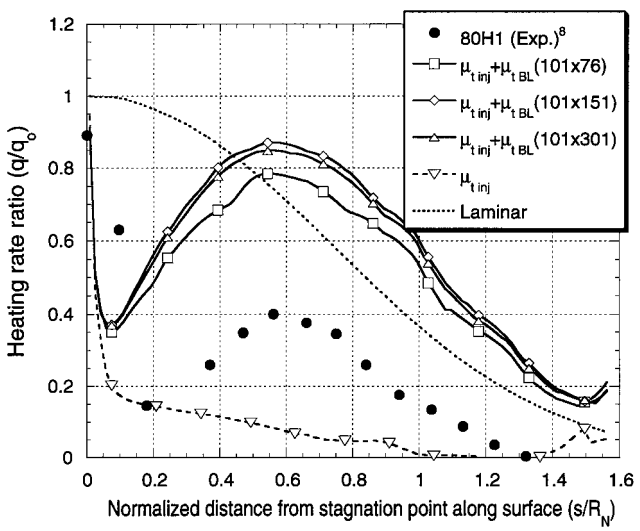

Fig. 4 Obtained heat-transfer-rate profiles by the new method.

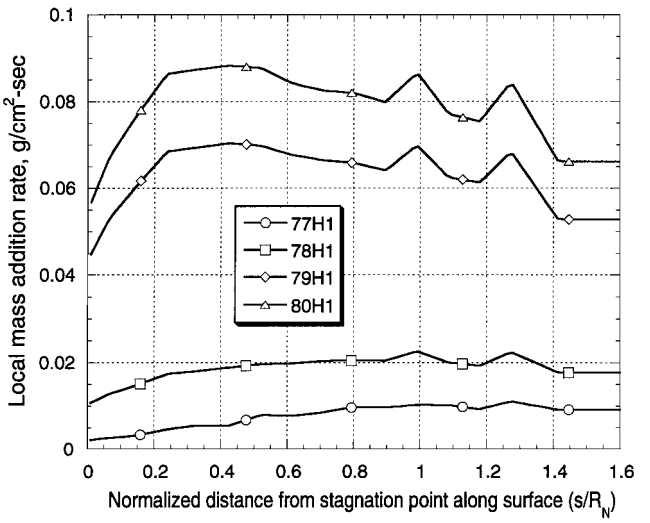

Fig. 5a Variation of mass addition rate along the wall surface for lower-Reynolds-number cases.

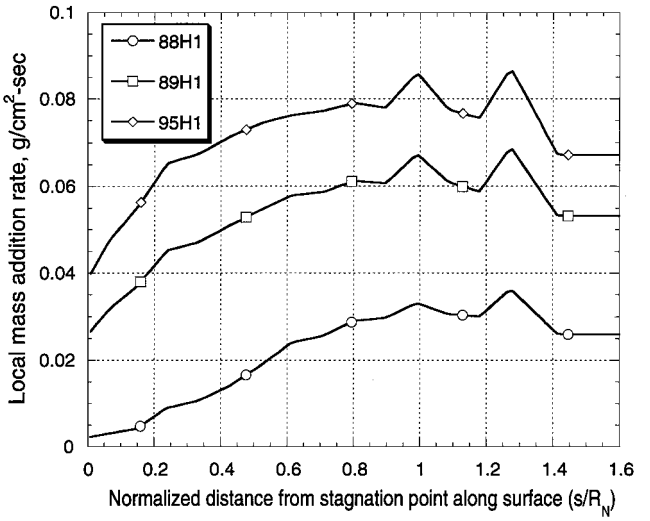

Fig. 5b Variation of mass addition rate along the wall surface for higher-Reynolds-number cases.

In Fig. 7a, which is reproduced from Fig. 11 in Ref. 8, the stagnation point heating rate ratio Ψ is shown for a different blowing parameter B that is the ratio of injected mass rate to the fraction of the maximum available heat arriving at the surface without mass addition.[21] A fair agreement between the calculated stagnation heating rates and the experiments for different Reynolds numbers is shown. In Ref. 10 Park calibrated his injection-induced turbulence model by several available experimental data including those shown in Fig. 7a. This agreement comes from the consistency between Park's theory and the present treatment of eddy viscosity in the numerical scheme. The polynomial curve $\Psi = \Psi(B)$ shown in the figure is obtained from the boundary-layer theory, which gives the correlation between the reductions in heat transfer with increasing mass addition parameter at the stagnation point.[21] Note that both the experimental data and the numerical results are substantially larger than the correlated curve.

The results of the larger blowing cases are also indicated in Fig. 7a for showing the behavior of the present numerical modeling to such cases, although we do not have the corresponding experimental data with which to compare. In these calculations the mass addition rate of model 80H1 is proportionally increased over the surface. As can be seen, the stagnation-point heating rate ratio gradually decreases as the blowing parameter is increased.

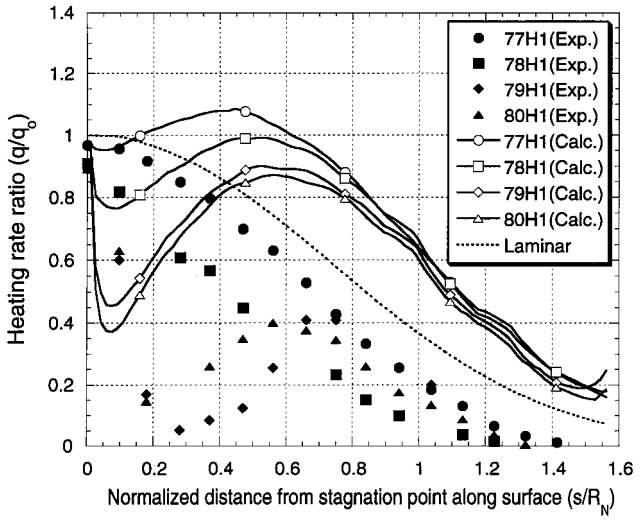

Fig. 6a Calculated heating-rate profile for lower-Reynolds-number cases.

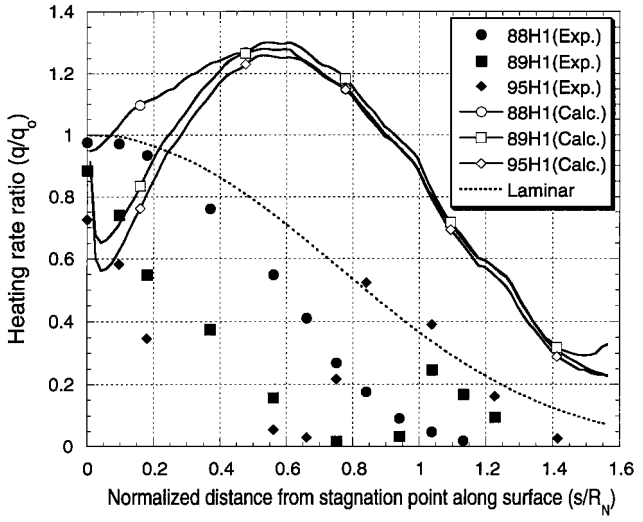

Fig. 6b Calculated heating-rate profile for higher-Reynolds-number cases.

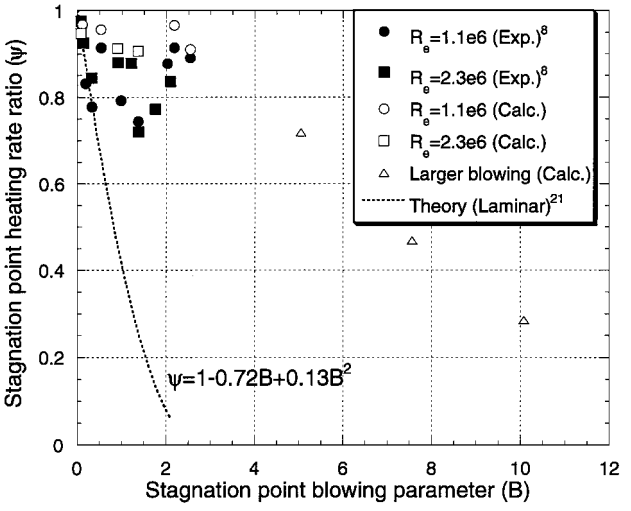

Fig. 7a Stagnation-point heating-rate ratio ψ for various blowing parameter B in Kaattari's experiment.[8]

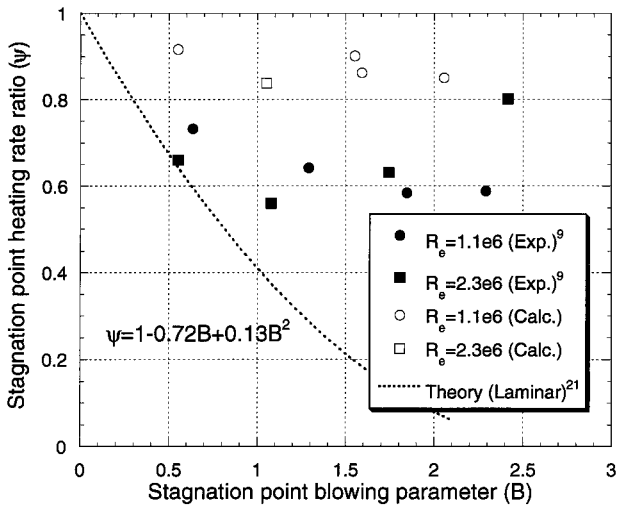

Fig. 7b Stagnation-point heating-rate ratio ψ for various blowing parameter B in Feldhuhn's experiment.[9]

Another set of experimental data for the normalized stagnation-point heat-transfer rate with surface mass addition is available in the literature[9] and is considered here as the source for further comparison. In the experiment a hemisphere-cone forebody made of porous beryllium-copper was utilized. In the calculations the time constant appearing in Eq. (3) is chosen to be 0.012 (Ref. 10). In Fig. 7b, which is reproduced from Fig. 18 in Ref. 9, the obtained stagnation-point heating-rate ratios are shown. One can find that the higher heating-rate ratio at the stagnation point is again reproduced, although the quantitative agreement is degraded in this case.

Further Attempts for Better Quantitative Agreement

The heating rates shown in Fig. 6 are obviously too large in the downstream region. Because the S–A model gave a better agreement in the downstream region, which was probably brought by the inconsistent use of destruction effect, it might give a better agreement if either the turbulence effect introduced by the associated turbulence model other than the S–A model could be diminished, or the turbulence effect at the stagnation point is artificially enhanced in the S–A model.

In the former approach the eddy viscosity in the Baldwin–Lomax model is decreased by modifying the mixing length as $d = C\chi y D$, where y is the distance from the wall and D is given by Eq. (6). The introduced constant is chosen in the range of $0 < C < 1$ so as to decrease the eddy viscosity in the boundary layer. This modification does not recover the original model when injection flow is absent. The current treatment is just for seeing the effect of diminishing eddy viscosity for surface heat transfer. Figure 8 shows the surface heating profiles corresponding to those shown in Fig. 6 with the arbitrarily chosen constant value $C = 0.5$. By reducing the mixing length, the agreements between the calculated profiles and experiments are improved.

In the latter approach we employ the S–A model as it is and add $(\mu_t)_{\text{inj}}$ [Eq. (8a)] only along the stagnation streamline. The obtained result is shown in Fig. 9. One can see that the agreement at the stagnation point is substantially improved. Moreover, the effect of added eddy viscosity has a sizable influence on the entire heating profile.

Discussion

In this study a new implementation of Park's injection-induced turbulence model into an existing computational fluid dynamics code is made to explore the surface heating rate over a hemispherical model with surface mass addition. The new implementation employs a direct use of mixing length theory with the modified Van Driest damping function, rather than resort to an existing turbulence model to introduce turbulence effect indirectly.

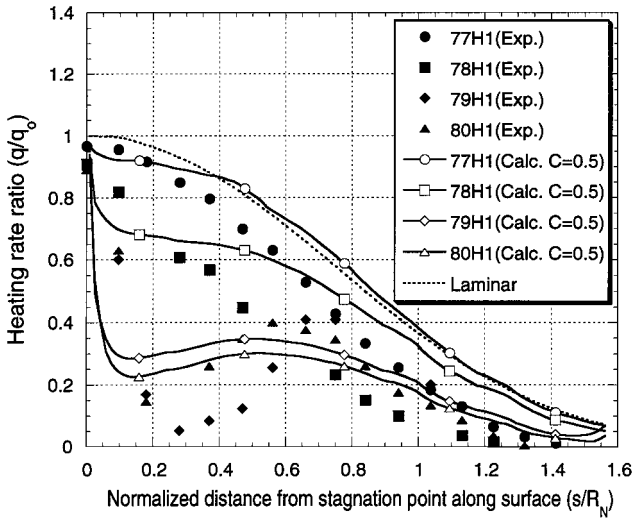

Fig. 8a Calculated heating-rate profile for lower-Reynolds-number cases by the reduced mixing length in the Baldwin–Lomax turbulence model.[20]

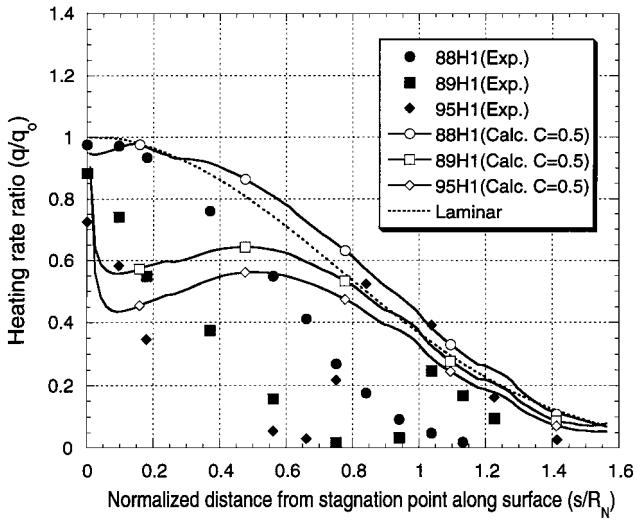

Fig. 8b Calculated heating-rate profile for higher-Reynolds-number cases by the reduced mixing length in the Baldwin–Lomax turbulence model.[20]

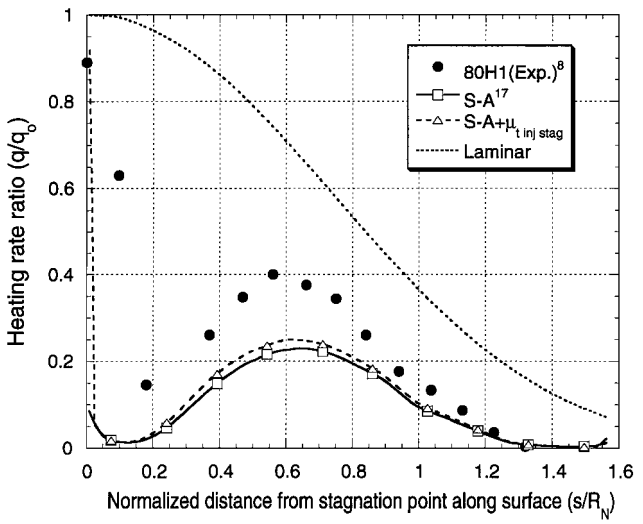

Fig. 9 Calculated heating-rate profile by the S–A model[17] with adding $(\mu_t)_{inj}$ only along the stagnation streamline.

As can be seen in the calculated results, particularly in Fig. 7, the enhanced surface heating at the stagnation point is well reproduced by the new method. Because the injection-induced turbulence model was developed for the purpose of explaining the anomalous heating enhancement at the stagnation point observed in various experiments involving the present one, any consistent numerical method with the Park's theory should reproduce the experimental values of the stagnation-point heating rate.

Contrary to this, the calculated surface heating rates by the associated turbulence models other than the S–A model consistently give higher values in the downstream region. Only the S–A model gives the favorable level of heating, although the destruction term in the S–A model is obviously inconsistent with the present turbulent injection assumption. Artificially diminished mixing length in the B–L model actually gives better coincidences in the downstream region while it does not alter the heating rate at the stagnation point. The introduction of $(\mu_t)_{inj}$ only along the stagnation streamline in the S–A model also improves the agreement.

From these results the suggestion is made that any of the following need to be considered for improved quantitative agreement: 1) an appropriate modification of Park's theory to reduce the amount of surface eddy viscosity caused by injection flow in the downstream region, 2) an appropriate modification of the mixing length in the existing turbulence models to reduce the amount of eddy viscosity in the downstream region, or 3) enhance the turbulence effect only at the stagnation region if the theory is implemented in the S–A turbulence model without modifying the near-wall destruction term.

Conclusions

Heat-transfer calculation for a hemisphere with wall injection in hypersonic flow is carried out by solving the axisymmetric Navier–Stokes equations. The injection-induced turbulence model of Park is implemented through a combination of two different eddy viscosity models, where the near-wall behavior of the turbulent injection gas is described by the ordinary mixing length theory using the modified Van Driest damping function, and the overall turbulent boundary layer is given by the Baldwin–Lomax zero equation model. What we have concluded in the present study are the following:

1) The heat-transfer rate at the stagnation point is reasonably well reproduced for various mass addition rates.

2) The injection-induced turbulence model needs to be combined with an appropriate turbulence model for reproducing transition phenomena.

3) The heat-transfer rate in the downstream region is found to be overestimated by the use of existing turbulence models. Suggestions are made for obtaining a better quantitative agreement in the downstream region.

References

[1]Fay, J. A., and Riddell, F. R., "Theory of Stagnation Point Heat Transfer in Dissociated Air," *Journal of the Aeronautical Sciences*, Vol. 25, No. 2, 1958, pp. 73–85.

[2]Ahn, H.-K., Park, C., and Sawada, K., "Dynamics of Pyrolysis Gas in Charring Materials Ablation," AIAA Paper 98-0165, Jan. 1998.

[3]Dorrance, W. H., *Viscous Hypersonic Flow*, McGraw–Hill, New York, 1962, pp. 39–68.

[4]Park, C., and Ahn, H.-K., "Stagnation-Point Heat Transfer Rates for Pioneer-Venus Probes," *Journal of Thermophysics and Heat Transfer*, Vol. 13, No. 1, 1999, pp. 33–41.

[5]Park, C., "Analytical Integration of Spallation Trajectories," *Proceedings of the Symposium on Shock Waves*, Saitama Univ., Saitama, Japan, 1997, pp. 461–464.

[6]Ahn, H.-K., and Park, C., "Preliminary Study of the MUSES-C Reentry," AIAA Paper 97-0278, Jan. 1997.

[7]Olynick, D. R., Chen, Y.-K., and Tauber, M. E., "Forebody TPS Sizing with Radiation and Ablation for the Stardust Sample Return Capsule," AIAA Paper 97-2474, June 1997.

[8]Kaattari, G. E., "Effects of Mass Addition on Blunt-Body Boundary-Layer Transition and Heat Transfer," NASA TP-1139, Jan. 1978.

[9]Feldhuhn, R. H., "Heat Transfer from a Turbulent Boundary Layer on a Porous Hemisphere," AIAA Paper 76-119, Jan. 1976.

[10]Park, C., "Injection-Induced Turbulence in Stagnation-Point Boundary Layers," *AIAA Journal*, Vol. 22, No. 2, 1984, pp. 219–225.

[11]Dendou, E., and Sawada, K., "Numerical Simulation of Hypersonic Flow over a Sphere with Surface Injection," AIAA Paper 98-0773, Jan. 1998.

[12]Demetriades, A., Laderman, A. J., Von Seggern, L., Hopkins, A. T., and Donaldson, J. C., "Effect of Mass Addition on the Boundary Layer of a Hemisphere at Mach 6," *Journal of Spacecraft and Rockets*, Vol. 13, No. 8, 1976, pp. 508, 509.

[13]Ahn, H.-K., Sawada, K., and Park, C., "CFD Calculation of Heat Fluxes in Turbulent Flow for Pioneer-Venus Probes," AIAA Paper 98-0833, Jan. 1998.

[14]Wakefield, R. M., and Pitts, W. C., "Analysis of the Heat-Shield Experiment on the Pioneer-Venus Entry Probes," AIAA Paper 80-1494, July 1980.

[15]Goldberg, U. C., and Ramakrishnan, S. V., "A Pointwise Version of Baldwin-Barth Turbulence Model," *Journal of Computational Fluid Dynamics*, Vol. 1, No. 4, 1993, pp. 321–338.

[16]Wada, Y., and Liou, M. S., "A Flux Splitting Scheme with High-Resolution and Robustness for Discontinuities," NASA TM-106452, Jan. 1994; also AIAA Paper 94-0083, Jan. 1994.

[17]Spalart, P. R., and Allmaras, S. R., "A One-Equation Turbulence Model for Aerodynamic Flows," AIAA Paper 92-0439, Jan. 1992.

[18]Cebeci, T., "Behavior of Turbulent Flow near a Porous Wall with Pressure Gradient," *AIAA Journal*, Vol. 8, No. 12, 1970, pp. 2152–2156.

[19]Van Driest, E. R., "On Turbulent Flow near a Wall," *Journal of the Aerospace Sciences*, Vol. 23, No. 11, 1956, pp. 1007–1011.

[20]Baldwin, B. S., and Lomax, H., "Thin Layer Approximation and Algebraic Model for Separated Turbulent Flows," AIAA Paper 78-257, Jan. 1978.

[21]Marvin, J. G., and Pope, R. B., "Laminar Convective Heating and Ablation in the Mars Atmosphere," *AIAA Journal*, Vol. 5, No. 2, 1967, pp. 240–248.